Real Time Adaptive Corrective Control of Short-Term Voltage Stability

Suárez, Estefanía A.Tapia; Graciela Colomé, D.; Rueda Torres, José L.

DOI
10.1109/ACCESS.2025.3643591

Publication date
2025

Document Version
Final published version

Published in
IEEE Access

IEEE Access
Multidisciplinary | Rapid Review | Open Access Journal

Received 16 November 2025, accepted 2 December 2025, date of publication 12 December 2025,
date of current version 31 December 2025.

Digital Object Identifier 10.1109/ACCESS.2025.3643591

RESEARCH ARTICLE

Real-Time Adaptive Corrective Control of Short-Term Voltage Stability

ESTEFANÍA A. TAPIA SUÁREZ[1], D. GRACIELA COLOMÉ[2], AND JOSÉ L. RUEDA TORRES[1], (Senior Member, IEEE)
[1]Department of Electrical Sustainable Energy, Delft University of Technology (TU Delft), 2628 AA Delft, The Netherlands
[2]Electrical Energy Institute, National University of San Juan, San Juan 5400, Argentina

Corresponding author: José L. Rueda Torres (j.l.ruedatorres@tudelft.nl)

This work was supported in part by German Academic Exchange Service (DAAD), and in part by the National Council for Scientific and Technical Research of Argentina (CONICET).

ABSTRACT Although several data-driven approaches for short-term voltage stability (STVS) assessment have been proposed, most of them do not extend to corrective control actions nor consider the joint dynamics of generation and load. To address this gap, this work introduces a real-time adaptive load shedding scheme (ALSS) driven by an integrated assessment of the short-term stability state (STSS) and the identification of critical induction motors (CIM) as the mechanism driving STVS instability. The methodology employs two recurrent convolutional neural network (RCNN) models operating in parallel: i) the STSS-RCNN, which classifies the system state as stable, unstable by transient stability (TS), or unstable by STVS; and ii) the CIM-RCNN, which identifies the critical motors responsible for instability, thereby inherently recognizing STVS-related problems. The joint operation of these models ensures that the ALSS is activated only when both responses consistently recognize an STVS event. This enables not only the correct activation of the load shedding scheme but also its accuracy and adaptive parameterization based on the identified CIMs. Validation on the IEEE 39-bus test system demonstrates that the proposed approach achieves robust real-time performance, outperforms single deep learning baselines, and significantly overcomes traditional load shedding schemes in efficiency and reliability.

INDEX TERMS Short-term voltage stability (STVS), load shedding scheme (LSS), induction motors, recurrent convolutional neural network (RCNN), phasor measurement units (PMU), real-time prediction.

I. INTRODUCTION

The increasing demands on power grids have led power systems to operate closer to their physical limits, conditions under which certain unanticipated disturbances can result in partial or even total system collapse. In particular, short-term voltage stability (STVS) has become a serious concern, as major collapses are associated with this type of instability [1]. Typically, STVS events occur in systems with a high concentration of dynamic loads, such as induction motors (IM), where the rapid acceleration of motors under a disturbance can cause a sharp voltage drop and exacerbate instability [2]. Load shedding schemes (LSS) have traditionally been used as emergency corrective actions due to their effectiveness, simplicity, and cost-efficiency [3], [4]. However, the LSS design to address STVS challenges is especially complex, given the intricate interactions among numerous system components and the fast transient dynamics that follow contingencies.

In this sense, an effective assessment of STVS is essential for the proper design and timely activation of an LSS that can adapt to system conditions. To achieve this adaptability, key parameters, such as the shedding location, amount, and execution time, must be dynamically tuned according to the severity of the STVS event. This assessment must be not only accurate, but also sufficiently fast to allow timely implementation of corrective control actions.

The associate editor coordinating the review of this manuscript and approving it for publication was Wen Chen.

To address the challenges of real-time STVS assessment, data-driven methodologies have gained significant attention. These approaches leverage both the high-resolution data provided by phasor measurement units (PMUs) and the rapid advancements in machine learning (ML), particularly deep learning (DL) techniques [5]. Using the large volumes of PMU data deployed across modern power systems, ML/DL-based methods are capable of learning complex nonlinear relationships, making them well suited for assessing STVS in real time. Some methodologies that have used ML methods include support vector machines (SVM) [6], artificial neural networks (ANN) [7], ensemble learning models (ELM) [8], and random forest (RF) [9]. These studies assess STVS with high accuracy, covering phenomena such as fault-induced delayed voltage recovery (FIDVR) and rapid voltage collapses. However, they require the development of carefully engineered features to construct effective representations of the input data for ML models. In other words, these methodologies are highly dependent on the manual and problem specific selection of features derived from domain knowledge and expertise.

In recent years, some advanced DL methods have been employed due to their ability to automatically extract fine grained features from large volumes of raw data without relying on intensive feature engineering. For instance, [10] proposes the use of long short-term memory (LSTM) networks to capture the temporal dependencies of electrical variables and predict the STVS state. Similarly, [11] exploits convolutional neural networks (CNNs) to predict fast voltage collapses by learning the spatial dependencies of voltage trajectories. To address the joint capture of spatial and temporal dependencies, hybrid architectures have been proposed. For example, [12] combines CNN and LSTM models to identify voltage instability and FIDVR phenomena using voltage trajectories within a short time window. Likewise, [13] employs graph convolutional networks (GCNs) together with LSTMs, enabling the extraction of complex spatio-temporal evolution patterns of STVS for prediction purposes. Furthermore, [14] introduces a spatio-temporal graph convolutional neural network (STGN) that integrates GCNs to incorporate network topology information for spatial learning, and 1D-CNN to extract temporal features, ultimately improving STVS assessment accuracy. More recently, [15], [16] have demonstrated that transformer based architectures achieve promising performance in capturing long range temporal dependencies and contextual information from post-fault PMU measurements, showing robustness under class imbalance and noisy conditions.

Despite the potential of the advanced algorithms for STVS assessment mentioned above, a fundamental limitation persists. Specifically, these methodologies do not fully account for the full spectrum of power system dynamics during the transient period, particularly the simultaneous interaction between generation and load dynamics [17], [18]. This omission undermines the accuracy and compromises the effective activation of corrective control actions.

There are a few studies that have attempted to incorporate both sides of this dynamic interplay in their assessments. These works aim to identify the dominant source of instability, i.e., whether it arises from synchronous generator (SG) out-of-step conditions (transient stability (TS)), or from IM stalling (STVS). For example, [19] introduces a two-dimensional index based on the double generation one-load (DGOL) model to quantify both the IM stalling margin and SG angle deviation margin. However, the accuracy of this approach heavily depends on extensive parameter tuning for specific contingencies, which limits its generalization.

Within the limited research that accounts for the joint dynamics of generation and load, [20] and [21] stand out for their use of ML and DL techniques to identify the primary driving force of instability. In [20], a decision tree-based classifier is employed to predict the short-term stability state (STSS) in real time (stable, unstable by TS, or unstable by STVS). Nevertheless, its training phase involves a computationally intensive offline process that requires calculating the unstable equilibrium point (UEP) to distinguish between the two instability mechanisms. In contrast, [21] avoids the need for complex mathematical formulations by introducing a direct and practical approach. It determines the dominant source of instability by selectively shedding either SG or IM components and observing the system's response. This procedure identifies whether instability arises from SG out-of-step (unstable by TS) or IM stalling (unstable by STVS). This insight is then used to train a robust DL model, specifically a recurrent convolutional neural network (RCNN) that integrates CNN and LSTM architectures. The trained model is capable of predicting the STSS in real time with high accuracy performance and robustness. Therefore, [21] provides a solid foundation for developing an advanced real-time control framework capable of executing automatic corrective actions to effectively mitigate transient phenomena.

In this context, the present work proposes an adaptive LSS (ALSS) to mitigate STVS events, building upon the assessment methodology introduced in [21]. Unlike conventional approaches, this study emphasizes the integration of assessment driven control actions, paving the way for the development of an effective control scheme. To support the proposed ALSS, this work introduces a complementary deep learning model, called CIM-RCNN, designed to identify the critical induction motors (CIM) responsible for voltage instability. Its architecture builds on the STSS-RCNN model from [21], leveraging its proven assessment capability while enhancing functionality toward control oriented decision making. The CIM offline identification is performed through a combination of stalling margin analysis and a shedding based ranking. Since both tasks, STSS assessment (Task 1) and CIM identification (Task 2) are closely related, the training of CIM-RCNN incorporates not only task specific data but also transfer learning from STSS-RCNN. This synergy improves learning efficiency and enables CIM-RCNN to achieve strong accuracy and generalization.

The insights provided by this model are essential for the ALSS parametrization, as it determines not only the location but also the amount of load to be shed in a timely manner. The main contributions of this work are as follows:

- Advancement of STVS analysis by integrating assessment and corrective control actions through an ALSS applied in real time.
- CIM-RCNN is introduced to identify the critical induction motors responsible for STVS events. This model integrates a dual stage offline analysis (stalling margin evaluation and a shedding based ranking), and leverages transfer learning from an existing STSS-RCNN model, leading to improved accuracy and generalization.
- The proposed ALSS can adapt its parameters (location, amount and time) according to STSS-RCNN and CIM-RCNN assessment results. This adaptive response ensures effective instability mitigation across a wide range of operating conditions and maintains strong performance even under partial data loss and measurement noise.

The remainder of this paper is organized as follows. Section II outlines the problems associated with data-driven STSS assessment and STVS control. Section III describes the proposed methodology developed to address these problems. Simulation results using the New England 39-bus test system are presented in Section IV. Section V provides a discussion of practical considerations associated with the proposed methodology. Finally, Section VI presents the conclusions of this work.

II. PROBLEM DESCRIPTION

The methodological framework described in [21] serves as the basis for the proposed ALSS aimed at mitigating STVS events. It relies on data-driven learning from a wide range of transient scenarios under failures conditions:

$$\mathcal{F} : x \rightarrow y, \quad \text{for } x = \{x_1, x_2, \ldots, x_B\}, \quad y \in \{0, 1, 2\} \quad (1)$$

where $x_i \in \mathbb{R}^{T \times d}$ $(1 \leq i \leq B)$ denotes the d-dimensional time series of bus system i among B buses considered during the early transient stages with T number of samples under a certain contingency. y represent the STSS classification label ($0 \rightarrow$ stable, $1 \rightarrow$ unstable by TS, $2 \rightarrow$ unstable by STVS).

In this context, x and y form an input-output pair for the STSS-RCNN model. In general, multiple variables can be incorporated into x based on their relevance to the problem to be detected and the observability of the system dynamics during the transient period. In this case, bus voltage magnitude, bus voltage angle, and IM speed $\{V, \theta, \omega\}$ are closely related to TS and STVS events and provide the necessary observability of transient dynamics. Therefore, they can be integrated into x ($x \in \mathbb{R}^{T \times B \times d}$, for $d = 3$). The variables data of $\{V, \theta\}$ can be directly obtained from PMU measurements, while the equivalent IM speed (ω) is assumed to be derived from IM parameters, voltage and current measurements [22], [23], [24].

The output y is determined by monitoring the rotor angle (δ), following a widely used transient stability criterion, and by applying full IM load shedding as a control action to help distinguish between transient and voltage instabilities.

$$y = \begin{cases} 0 & \text{if } |\Delta\delta|_{\max} < 180^\circ \text{ under no control action} \\ 1 & \text{if } |\Delta\delta|_{\max} > 180^\circ \text{ under IM load shedding} \\ 2 & \text{if } |\Delta\delta|_{\max} < 180^\circ \text{ under IM load shedding} \end{cases} \quad (2)$$

where $|\Delta\delta|_{\max}$ is the largest absolute rotor angle separation between any generator with respect to the reference generator during the transient period [25].

In this way, the STSS-RCNN model, through the underlying mapping function $\mathcal{F}$, is capable of providing a fast assessment of system's stability state. Once the system is identified to be unstable, specifically due to STVS, corrective control actions involving IM load shedding should be taken as soon as possible to stabilize the system. Although full IM load shedding can restore system stability, it is often excessively conservative in practice and may lead to unnecessary disruption. The impact of IMs on system stability varies depending on the operating scenario and the contingency. Therefore, adaptively selecting and shedding only the most critical IMs (CIM) would be the most efficient approach to system stabilization.

The successful implementation of IM load shedding actions for system stabilization can be achieved by reliable identifying CIM. Similar to the previously data-drive STSS assessment, online CIM can also be performed in a data-driven manner. Specifically, this is achieved through a vectorized output $\boldsymbol{Y} = [Y_1, Y_2, \ldots, Y_{n_m}]$, where n_m is the number of motors, and each element $Y_j \in \{0, 1\}$ $(1 \leq j \leq n_m)$ indicates the motor j criticality state label ($0 \rightarrow$ non critical, $1 \rightarrow$ critical). A new mapping $\mathcal{G} : x \rightarrow \boldsymbol{Y}$ can be learned by exploring numerous transient scenarios. This mapping results in a data-driven CIM-RCNN model, which complements the STSS-RCNN model and works similarly and in parallel during online application. The implementation of both RCNN models enables not only accurate detection of STVS issues but also the identification of the location and quantity of IM loads to be shed, facilitating the configuration of an adaptive LSS aimed at mitigating STVS problems. More details about the whole approach are presented in Section III.

III. METHODOLOGY

The overall framework of the integrated methodology of STSS assessment and CIM identification is illustrated in Fig. 1. The methodology includes three phases which are detailed below.

A. DATABASE GENERATION

The database, constructed over a base topology consists of: i) input data x, corresponding to time series response of $\{V, \theta, \omega\}$; and ii) STSS and CIM labeling.

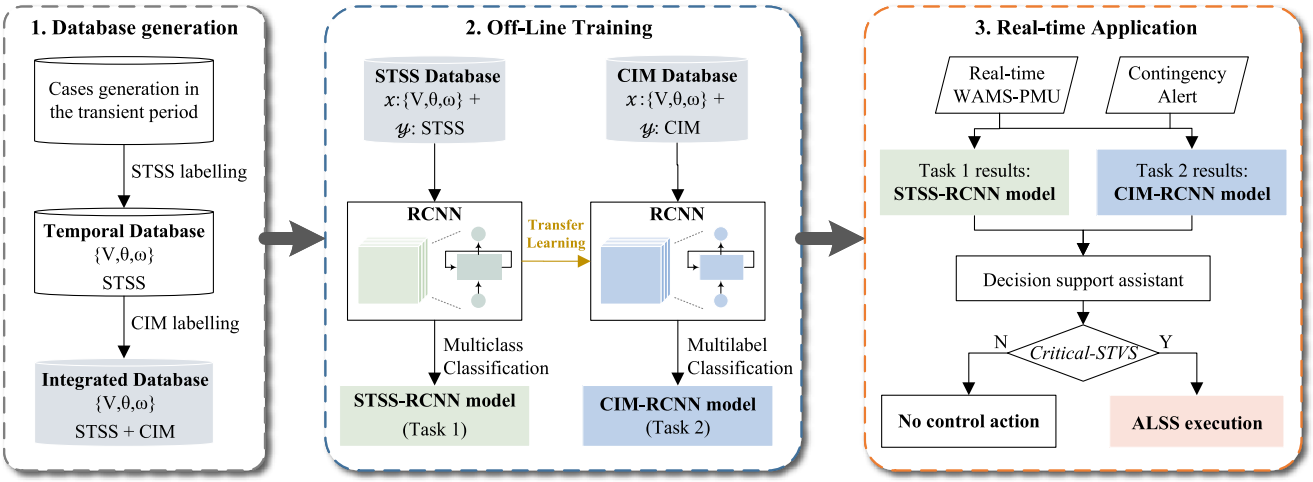

FIGURE 1. Overall framework of the STSS assessment and STVS control methodology.

1) TIME SERIES DATA

The time series data of $\{V, \theta, \omega\}$ are obtained by considering a wide spectrum of operating scenarios and n-1 contingencies. Uncertainties are introduced in: the type of contingency (generator outage or three-phase short circuit in a transmission line), the failure component, the fault location (generator or line, and the percentage of the line length where the fault occurs), and the load/generation scenario. To account for these uncertainties, a Monte Carlo (MC) simulation framework was employed, in which the input parameters were randomly sampled according to their associated probability distributions [26].

Within this framework, the acquisition of time series data is as follows [26]: 1) construction of random load scenarios using probability distribution functions and short-term demand forecasting; 2) calculation of the optimal power flow and determination of generator dispatch; 3) random selection of an n-1 contingency; 4) selection of line or generator; 5) execution of time-domain dynamic simulation; and 6) storage of the resulting time series data of $\{V, \theta, \omega\}$ from the beginning of the contingency t_0 to an early time window t_w, comprising T number of samples with a time step Δt according to the PMU sampling interval.

This stochastic process enables the generation of a large and diverse set of operating and failure conditions, ensuring a comprehensive representation of the system behavior under different scenarios and thereby enhancing the generalization capability of the proposed STSS-RCNN and CIM-RCNN models.

2) STSS AND CIM LABELING

The STSS labeling y is determined following (2). Specifically, a time window (TW) and a control action time t_{ac} for the IM load shedding are defined, enabling the identification of the instability type. Note that, TW corresponds to a time length which short-term problems, STVS or TS, could develop.

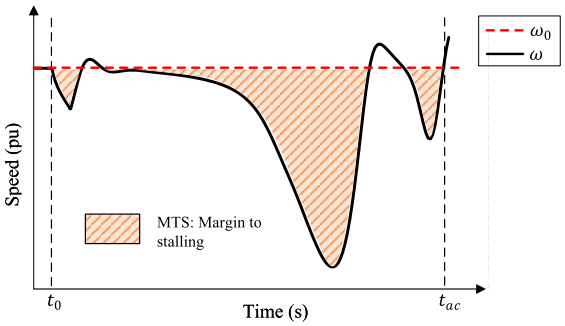

FIGURE 2. IM speed response under a disturbance and MTS definition.

Regarding the CIM labeling, the multilevel vector Y is derived here. This vector indicates which motors are considered critical; that is, which motors, when disconnected, enable the system to restore STVS. To this end, a practical methodology is proposed in which IM load shedding control actions are executed based on the stalling tendency of each IM. Specifically, inspired by [19], the method calculates the margin to stalling (MTS) for each motor, ranks them from highest to lowest, and performs load shedding accordingly. Motors whose disconnection allows the system to improve its stability are identified as CIMs.

The MTS index quantifies the speed deviation exhibited by a motor in response to a disturbance. A higher MTS value indicates a greater deviation and, consequently, a higher consumption of reactive power from the grid, making the system more susceptible to be unstable by STVS. Fig. 2 illustrates the behavior of a motor speed (ω) under a disturbance. The MTS corresponds to the shaded area, defined by the deviation of the motor speed relative to its pre-fault value (ω_0) over the time interval from the

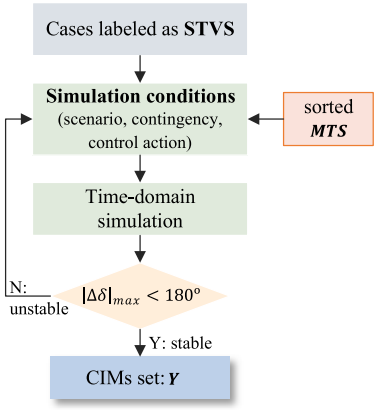

FIGURE 3. Methodology flowchart for CIMs identification.

disturbance starts (t_0) to the moment when control actions are executed (t_{ac}). Since all motor speeds are expressed in per-unit (pu), the MTS remains comparable across the different IMs. The MTS is defined as follows:

$$MTS = \int_{t_0}^{t_{ac}} MTS(t)\, dt \tag{3}$$

$$MTS(t) = \begin{cases} \dfrac{\omega_0 - \omega(t)}{\omega_0} & \text{if } `\omega(t) < \omega_0 \\ 0 & \text{else} \end{cases} \tag{4}$$

The MTS index is computed for each IM in the system, resulting in a vector $\boldsymbol{MTS} = [MTS_1, MTS_2, \ldots, M_{n_m}]$. The elements of this vector are sorted in descending order, revealing the criticality of each motor and serving as input for CIM identification. The procedure used for this identification is illustrated in Fig. 3.

As shown in Fig. 3, only the cases labeled as unstable by STVS, according to (2), are considered. For each case, the simulation conditions (operating scenario and contingency) are adjusted. At this stage, the IM to be disconnected is also selected based on the sorted $\boldsymbol{MTS}$, using t_{ac} as the control action time. A time-domain simulation is then performed to assess the system response. If the system recovers through this control action ($|\Delta\delta|_{\max} < 180°$), it indicates that disconnecting only the selected IM is sufficient to restore STVS stability. In this case, this motor is identified as a CIM. Conversely, if the system fails to recover, the process is repeated by adding the next IM in the sorted $\boldsymbol{MTS}$ to the shedding set. This iterative procedure continues until the minimum set of CIMs required to restore stability is identified. In this way, the number of CIMs is determined based on the instability severity, enabling the adaptability of the proposed ALSS. It is important to note that the CIM set defines the vector $\boldsymbol{Y}$ for STVS cases, whereas for cases classified as either stable or unstable by TS, all elements of $\boldsymbol{Y}$ are zero, as there are no critical motors.

Once the data $\{x, y, \boldsymbol{Y}\}$ are obtained for each transient case, an integrated dataset is prepared for training both the STSS-RCNN and CIM-RCNN models in the second phase.

B. OFF-LINE TRAINING

Complex spatial and temporal correlations emerge in the short-term dynamics of power systems. Therefore, a model capable of capturing these features from wide-area system behavior is essential for both STSS assessment (Task 1) and CIM identification (Task 2). In this context, a hybrid RCNN learning model is proposed to perform these tasks. By combining hierarchical CNN and LSTM modules, the model effectively learns spatial and temporal patterns across the system, while also offering high performance, robustness, and strong generalization capability. The basic architecture of the RCNN is shown in Fig. 4, where its description and implementation for both Task 1 and Task 2 are described below.

1) RECURRENT CONVOLUTIONAL NEURAL NETWORK

As shown in Fig. 4, by mapping the system wide area dynamics through multi-dimensional time series data organized into grid-like structure (x), the RCNN model is able to extract spatial features via the CNN module and temporal features via the LSTM module. The RCNN architecture also includes a flatten layer, fully connected (FC) layers, and a classifier. The flatten layer transforms the multidimensional outputs into a one-dimensional feature vector suitable for processing by the FC layers. The FC layers integrate and relate the extracted features. Finally, the classifier performs the discrimination of STSS (y) or CIM ($\boldsymbol{Y}$).

- *Convolutional Neural Network - CNN Module*
  This module focuses on learning spatial features from multidimensional data through convolution operations. It employs k convolutional filters, each applied across different channels to map features. The output of the l-th convolutional layer is given by $q_l = f_a(k_l, x_l)$, where x_l, k_l, and q_l represent the input feature map, the convolution kernel, and the hidden feature map at iteration l, respectively, and f_a denotes the activation function [27].
  The CNN module captures hidden features using pooling for down sampling, shared weights for computational efficiency, dropout techniques to mitigate overfitting commonly encountered in deep networks, and batch normalization (BN) to stabilize and accelerate training by normalizing layer inputs [27].
- *Long-Short Term Memory - LSTM Module*
  LSTM is a widely used variant of recurrent neural networks (RNNs), known for its effectiveness in capturing temporal dependencies in sequential data. It addresses the vanishing gradient problem common in traditional RNNs, enabling stable training over long sequences [28].
  The LSTM cell uses three gates (input, forget, and output) to control the flow of information, allowing the network to retain or discard temporal features as needed. At each time step t, the input x_t, cell state c_t, and hidden state h_t interact through nonlinear

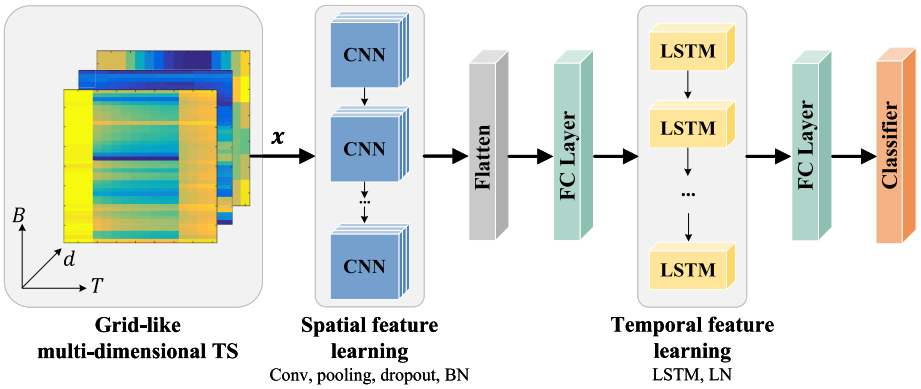

FIGURE 4. Basic architecture of RCNN.

transformations governed by the activation function σ. Often, layer normalization (LN) is applied within LSTM cells to stabilize and accelerate training by normalizing the inputs across features, improving generalization and convergence speed [28].

2) RCNN FOR STSS ASSESSMENT

Essentially, this task belongs to a multiclass classification problem. Therefore, the classifier uses the softmax function to obtain the following numerical prediction y_p of the STSS for the class c:

$$y_{pc} = \frac{e^{z_c}}{\sum_s e^{z_c}}; (c = 1, 2, 3) \tag{5}$$

where $y_{p1} + y_{p2} + y_{p3} = 1$, and z_c corresponds to the vector of predictive values for the class c. Additionally, the weighted cross-entropy (WCE) loss function is employed for the training. This approach effectively addresses the class imbalance problem (more stable than unstable samples), improving both model fitting and generalization. The per-sample learning objective is defined as:

$$\min \mathcal{L}_{STSS} = \min[-\alpha \sum\nolimits_c (y_c \log y_{pc})] \tag{6}$$

where α is the balanced factor. In practice, a higher value is assigned to the unstable classes, since they contain fewer samples.

The predicted output y_p can be taken as a probabilistic value, which reveals the probability of keeping stability in the transient period. In this sense, the STSS is predicted as:

$$\tilde{y} = \begin{cases} 0 \text{ (stable)} & \text{for } y_{p1} > 0.5, \\ 1 \text{ (unstable TS)} & \text{for } y_{p2} > 0.5, \\ 2 \text{ (unstable STVS)} & \text{for } y_{p3} > 0.5. \end{cases} \tag{7}$$

According to (7), when the probability of one of the classes exceeds the threshold of 0.5, the STSS prediction is assigned to that class.

3) RCNN FOR CIM IDENTIFICATION

Unlike Task 1, the RCNN for CIM identification addresses a multi-label classification problem, in which each sample is associated with a set of labels. Each label is assigned a binary code 0/1 to represent False/True, allowing the problem to be decomposed into multiple related binary category learning [29]. The classifier employs the sigmoid function, which produces a numerical prediction vector $\boldsymbol{Y_p}$, indicating the probability of all labels. When the probability for the label $Y_{pj} > 0.5$, that label is predicted to be true. In this case, each label corresponds to a motor, and the set of labels composes the output prediction vector $\tilde{\boldsymbol{Y}}$, indicating the state of each motor as true (critical) or false (non-critical). The subset of true labels refers to the predicted critical motors CIM_p.

Regarding the training, the WCE loss is extended to the multi-label setting, treating each label as an independent binary task. Therefore, the per sample learning objective is defined as follows:

$$\min \mathcal{L}_{CIM} = \min[-\alpha(\sum_{j=1}^{j=n_m} Y_j \log Y_{pj} + (1 - Y_j) \times \log(1 - Y_{pj})) + R] \tag{8}$$

An R regularization term is included to prevent overfitting and enhance generalization. This term is defined as:

$$R = \frac{1}{2}\beta \left(\|\mathbf{w}\|^2 + \|\mathbf{b}\|^2 \right) \tag{9}$$

where $\mathbf{w}$ and $\mathbf{b}$ are learnable network parameters, and β is the regularization weight. The objective functions formulated in Task 1 and Task 2 are optimized using the Adam algorithm, a widely adopted method in DL that leverages adaptive learning rates (lr) and momentum to achieve fast and stable convergence [30].

4) STSS-RCNN AND CIM-RCNN DESIGN

Given the strong relationship between STSS assessment and CIM identification, particularly when STSS is unstable by STVS, the design of both models, STSS-RCNN and CIM-RCNN, is proposed to be highly similar. The goal is for

TABLE 1. Confusion matrix for a binary classification problem.

	Actual stable	Actual unstable
Predicted stable	TP (true positive)	FP (false positive)
Predicted unstable	FN (false negative)	TN (true negative)

one model to support the other during the learning process, thereby enhancing classification performance. In this context, Task 2 is significantly more complex than Task 1, as it involves a larger number of labels. Therefore, the model developed for Task 1 is employed to support the model in Task 2. To achieve this, the transfer learning technique is leveraged, which consists of reusing the knowledge acquired during the training of one task in another closely related task, resulting in substantial performance improvements when a strong correlation exists between them [29].

In this sense, STSS-RCNN is trained first, and its spatial feature parameters from the CNN module are then transferred to CIM-RCNN. During the training for Task 2, these parameters are kept frozen, preventing any updates, and thereby serving as a stable reference for guiding the optimization of the remaining parameters. This approach allows the CIM-RCNN to benefit from the spatial feature representations already learned in Task 1, accelerating convergence and improving generalization.

5) PERFORMANCE METRICS

As STSS-RCNN and CIM-RCNN perform different types of classification (multiclass and multi-label), two categories of metrics are used to measure their performance.

- *Confusion matrix based metrics (STSS-RCNN)*
  Based on the confusion matrix presented in Table 1 for binary classification problems, performance metrics such as accuracy (Acc), security (Ss), reliability (Cu), and G-mean can be adopted to measure the STSS-RCNN. Although the STSS-RCNN addresses a multiclass classification problem, each class c can be reformulated as a binary subproblem, allowing the calculation of these metrics as defined in (10) - (13).

$$\text{Acc} = \frac{TP + TN}{TP + FP + TN + FN} \tag{10}$$

$$\text{Ss} = \frac{\sum_c \frac{TP_c}{TP_c + FN_c}}{c_T} \tag{11}$$

$$\text{Cu} = \frac{\sum_c \frac{TN_c}{TN_c + FP_c}}{c_T} \tag{12}$$

$$G\text{-mean} = \sqrt{\text{SS} \times \text{CU}} \tag{13}$$

  where c_T denotes the total number of classes. Acc is a widely used metric, as it provides an overall measure of the proportion of correctly predicted samples. Ss represents the proportion of correctly classified samples among all stable samples. Cu represents the proportion of correctly classified samples among all unstable samples, reflecting the reliability of the system assessment. Finally, $G-$ mean is a suitable metric for assessing classification performance on imbalanced samples [29].
- *Set similarity based metrics (CIM-RCNN)*
  Since CIM-RCNN outputs a vector $\tilde{\boldsymbol{Y}}$ composed of labels indicating the predicted state of each motor as either critical or non-critical, the model evaluation in this case must be based on set similarity. Therefore, the Jaccard index is employed, as it measures the similarity between two sets of integers [31]. Given two sets A and B, the Jaccard index is defined as follows:

$$\text{J}(A, B) = \frac{|A \cap B|}{|A \cup B|} = \frac{|A \cap B|}{|A| + |B| - |A \cap B|} \tag{14}$$

  where $\text{J} \in [0, 1]$. In this case, a sample is considered correctly classified when $\text{J}(Y, \tilde{\boldsymbol{Y}}) = 1$. Similar to Acc and Cu metrics described above, Jaccard accuracy (JACC) and Jaccard accuracy for unstable (JACCU) samples are defined to evaluate performance across all samples and unstable samples, respectively. Additionally, Jaccard effectiveness for unstable (JACCEU) samples is also defined to evaluate whether the identification of CIM in unstable samples is sufficient to mitigate STVS instability. If the CIM-RCNN model identifies more motors than necessary, instability can still be prevented by disconnecting even the surplus motors.

C. REAL-TIME APPLICATION

Once the STSS-RCNN and CIM-RCNN models have been trained and their performance evaluated, they are available for real-time application. During this application, when the system encounters a transient contingency n–1, real-time data $\{V, \theta, \omega\}$ are acquired from the system buses B. This data is assumed to be collected from the moment the fault occurs until an early time t_w, spanning a few T time steps. The resulting measured data $x \in \mathbb{R}^{T \times B \times 3}$ are then fed into each trained model for their respective predictions $(\tilde{y}, \tilde{\boldsymbol{Y}})$. These predictions are integrated by a decision support assistant (DSA) to produce a logical and consistent response of the system final stability state. If the DSA output is *critical* $-$ *STVS*, the ALSS is activated, and its adjustment parameters (location and quantity) are adjusted based on the motors identified as critical in $\tilde{\boldsymbol{Y}}$. The operation of the DSA and ALSS are detailed below.

1) DECISION SUPPORT ASSISTANT DSA

The DSA is implemented to logically integrate the prediction outputs of the STSS-RCNN and CIM-RCNN models, enabling the proper activation and parameter setting of the ALSS. In this sense, the DSA is defined as:

$$\text{DSA} = \begin{cases} \textit{safe} & \text{if } \tilde{y} = 0 \ \ \& \ \ \tilde{\boldsymbol{Y}} = \emptyset \\ \textit{critical}-\textit{TS} & \text{if } \tilde{y} = 1 \ \ \& \ \ \tilde{\boldsymbol{Y}} = \emptyset \\ \textit{critical}-\textit{STVS} & \text{if } \tilde{y} = 2 \ \ \& \ \ \tilde{\boldsymbol{Y}} \neq \emptyset \\ \textit{inconsistent} & \text{else} \end{cases} \tag{15}$$

As shown in (15), the DSA provides four possible final state outputs:

- *Safe*: This output occurs when the STSS-RCNN prediction is stable ($\tilde{y} = 0$) and the CIM-RCNN prediction is an empty vector ($\tilde{\boldsymbol{Y}} = \emptyset$), meaning that no motor is identified as critical. Both results are consistent, since under stable conditions no critical motor is present.
- *Critical - TS*: This final state occurs when the STSS-RCNN predicts the system as unstable by TS ($\tilde{y} = 1$) and, at the same time, the CIM-RCNN predicts an empty vector ($\tilde{\boldsymbol{Y}} = \emptyset$), meaning that no motor is identified as critical. In this case, both predictions are consistent, since in transient instability problems, the load is not part of its mechanism.
- *Critical - STVS*: This DSA output is obtained when the STSS-RCNN predicts the system as unstable by STVS ($\tilde{y} = 2$) and the CIM-RCNN predicts a non-empty vector ($\tilde{\boldsymbol{Y}} \neq \emptyset$), indicating that critical motors have been identified. These predictions are consistent, as STVS problems involve motors in a critical state that directly contribute to the instability development.
- *Inconsistent*: This DSA output means that there is a mismatch between the predictions of the two models. For example, this occurs when the STSS-RCNN predicts the system as stable or unstable due to TS, but the CIM-RCNN identifies critical motors; or when the STSS-RCNN predicts instability due to STVS, but the CIM-RCNN does not identify any motor as critical. These cases indicate a lack of coherence between the STSS classification and the CIM identification, which may arise from model misclassifications, measurement noise, or atypical system dynamics.

2) ADAPTIVE LOAD SHEDDING SCHEME-ALSS

The ALSS will be activated only when the DSA output is *critical – STVS*, with parameters set from the CIM-RCNN prediction, giving the scheme adaptive characteristics. The parameter setting procedure is detailed below.

- *Load shedding: location and amount*
  These two parameters are set based on the critical motors predicted by the CIM-RCNN (CIM_p), as each motor inherently contains information about its location and load consumption. Specifically, the motors are located at buses locations $\boldsymbol{b} = [b_1, b_2, \ldots, b_{n_m}]$ with corresponding load consumption $\boldsymbol{P} = [P_1, P_2, \ldots, P_{n_m}]$. Therefore, when a motor j is predicted as critical, the parameter setting is defined by (16) and (17).

$$LS_{location} = b_j, \text{ for } j \in CIM_p \tag{16}$$

$$LS_{amount} = \sum\nolimits_j P_j, \text{ for } j \in CIM_p \tag{17}$$

- *Load shedding: time*
  The motor load shedding time is determined based on the latencies involved in applying real-time control actions. This includes computation delay, PMU data acquisition, communication latency, activation signal transfer, circuit breaker operation, and the STSS-RCNN and CIM-RCNN operation (t_w). Among these time delays, the only adjustable parameter is the time window t_w required by the RCNN models to perform STSS assessment and CIM identification. The remaining latencies depend on external factors, such as technological advancements and computational capacity. Therefore, the t_w length for both models must ensure that control actions are executed with sufficient anticipation to prevent instability, while maintaining high classification performance by the models.

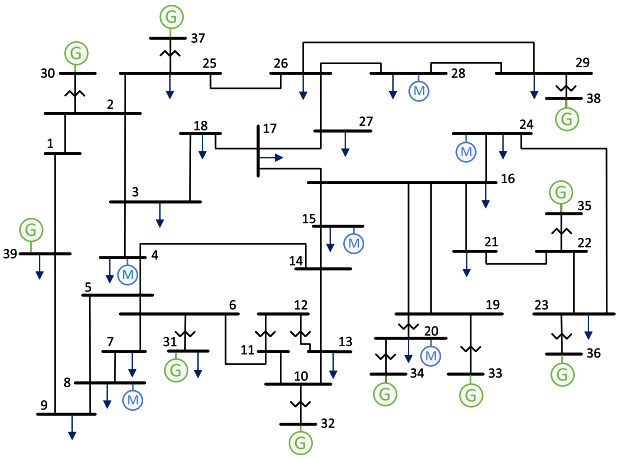

FIGURE 5. IEEE New England 39-bus system.

IV. SIMULATION RESULTS

The proposed methodology was tested on the modified New England 39-bus system that satisfies n-1 security criterion [32]. The database was generated in DIgSILENT PowerFactory, and the RCNN models were developed in Python using Keras and TensorFlow libraries on a computer with an Intel Core i7-9750H @ 2.60 GHz and 16 GB RAM.

A. SYSTEM DESCRIPTION AND SIMULATION SETTINGS

The New England 39-bus system comprises 39 buses, 10 generators, 19 loads, and 46 transmission lines, and was modeled with the dynamics of both generation and loads. Power plants were modeled as 6th-order generators equipped with automatic voltage regulators and speed control regulators. Induction motors were modeled using IEEE Type 2 dynamic loads, which were located at 6 different buses as shown in Fig. 5. Generators and motor loads are modeled with different ratings as described in [26].

The time-domain dynamic simulations were generated under the following aspects:

- Contingencies of generation outages and three-phase faults randomly located on transmission lines, with fault occurrence at $t_0 = 0.1$ s and fault clearance at $t_c = 0.2$ s (fault duration $t_f = 0.1$ s).

TABLE 2. Summary of hyperparameter settings for the RCNN models.

Hyperparameters	STSS-RCNN	CIM-RCNN
Weighting factors	$\alpha = [0.5, 3, 8]$	$\beta = 0.005$
Optimization algorithm	Adam, lr = 0.0001	Adam, lr = 0.0001
Initialization	Glorot uniform	Glorot uniform
Batch size	120	120
Epochs	2000	2000

- The PMU sampling interval was set to $\Delta t = 0.01$ s, and it is assumed that PMUs were available at all system buses.
- For labeling $(y, \boldsymbol{Y})$, the control action time was set to $t_{ac} = 0.5$ s (0.3 s after fault clearance). This setting accounts for both real-time control action latencies ($t_L = 0.26$ s [33], [34], [35]) and the RCNN models operation time ($t_W = 0.14$ s). The latter includes the fault duration ($t_f = 0.1$ s) and an additional time margin ($t_m = 0.04$ s) to allow the models to develop high performance while maintaining timely prediction.
  The labeling was conducted within a time window $TW = 5$ s, where STVS and TS problems may develop.
- For input data (x), in each sample it was assumed that the system responses of $\{V, \theta, \omega\}$ at the 39 buses were obtained or estimated from the acquisition of PMU data. Note that, for buses without induction motors, the speed values (ω) were set to 0.
  The time length data collection for the RCNN models ($t_W = 0.14$ s) comprises $T = t_W/\Delta t + 1 = 0.14/0.01 + 1 = 15$ samples. Thus, the multi-dimensional time series data are arranged in the form $x \in \mathbb{R}^{15\times 39\times 3}$.

Based on these aspects, 10000 transient samples were generated, consisting of the input vector x and corresponding labels $(y, \boldsymbol{Y})$. This database size is considered sufficient to properly train the learnable parameters of the RCNN models, as well as to ensure reliable assessment performance assessment for both STSS and CIM.

The database was divided into three groups: training (60% ≡ 6000 samples), validation (20% ≡ 2000 samples), and testing (20% ≡ 2000 samples); where the percentage of stable, unstable by TS, and unstable by STVS in each set has the same proportionality.

B. RCNN MODELS DESIGN

The design of the STSS-RCNN and CIM-RCNN models involves comparing groups of hyperparameters to achieve high classification performance and generalization capability. In this context, different groups of hyperparameters were compared, and the one yielding the best results was selected. Table 2 summarizes the final hyperparameter settings, while the remaining architectural choices are illustrated in Fig. 6. As shown, the CNN module of CIM-RCNN (Fig. 6b) shares the same architecture as STSS-RCNN (Fig. 6a), since this stage involves knowledge transfer.

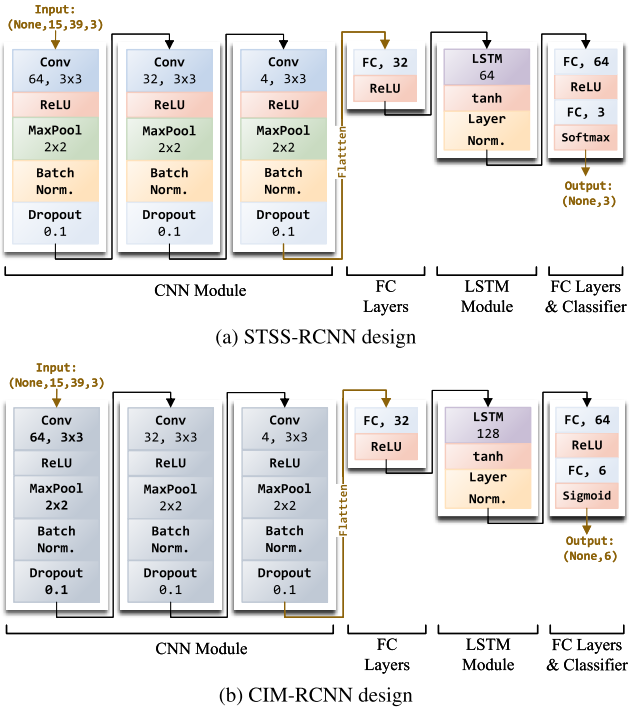

FIGURE 6. Architectural design of the RCNN models.

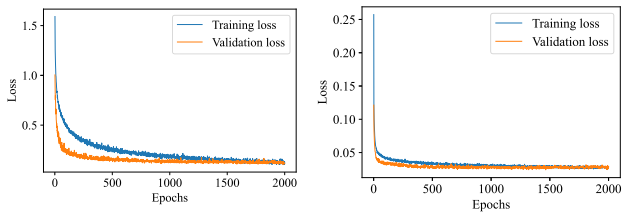

FIGURE 7. Training loss and validation loss of STSS-RCNN and CIM-RCNN during the training process.

On the other hand, the generalization capability of the models can be verified through the convergence of the training and validation losses toward a stable point, where neither overfitting nor underfitting is observed. Fig. 7 illustrates the learning process for both models, confirming that proper training was achieved, showing strong generalization capability.

C. PERFORMANCE EVALUATION

Once both models, STSS-RCNN and CIM-RCNN, are properly trained, their performance is evaluated using the previously introduced metrics. The results are summarized in Table 3, and their analysis is presented below.

1) PERFORMANCES ON STSS ASSESSMENT AND CIM IDENTIFICATION

Clearly, as shown in Table 3, both classification tasks achieve high performance levels on the training and test datasets.

TABLE 3. Performance results.

	Task 1: STSS-RCNN				Task 2: CIM-RCNN		
Dataset	Acc	Ss	Cu	Gmean	Jacc	Jaccu	Jacceu
Training	98.32	98.15	99.77	98.96	99.08	97.73	98.91
Test	98.20	98.09	99.26	98.67	98.87	97.60	98.60

In the case of the STSS-RCNN model, the metrics Cu and *G*mean are of particular interest, as they highlight the model's ability to correctly detect unstable samples in an imbalanced dataset with a low proportion of such cases. In this case, Cu and *G*mean exceed 99% and 98.5%, respectively, indicating that the model can accurately identify unstable samples, including those related to STVS, and thus enables the correct activation of the ALSS through the DSA module.

On the other hand, the CIM-RCNN model also demonstrates strong performance, with Jacc and Jacceu values above 98.5% and Jaccu close to 98%. Although Jaccu shows slightly lower performance compared to the other metrics, this result indicates that in 97.6% of the unstable samples the same critical motors as those considered true are correctly identified. In contrast, Jacceu achieves higher performance, showing that in 98.6% of the unstable samples the motors identified as critical (although in greater number than the true ones) would lead the system stabilization.

Based on the results of both models, the DSA module evaluates their responses, allowing the effective application of CIM-based remedial control actions (ALSS). To illustrate this, two cases randomly selected from the test dataset are presented below. In these cases, the STSS-RCNN model classified them as unstable due to STVS, while the CIM-RCNN model identified critical motors. Consequently, the DSA module generates a *critical-STVS* response, leading to the activation of the ALSS. Fig. 8 and 9 show the voltage profiles of all system buses, with and without the application of control actions, for two different 3-phase faults on transmission lines 17–18 and 14–15 in Fig. 5.

As shown in Figs. 8(a) and 9(a), both examples exhibit unstable responses. Although the voltages initially attempt to recover after the fault clearance, they quickly decay into subsequent oscillations, ultimately leading to system collapse. The STSS-RCNN model successfully predicts the system' state as unstable by STVS, while the CIM-RCNN model identifies critical motors. In the first case, Fig. 8(b), a single critical motor is present and correctly identified by the CIM-RCNN model. In the second case, In Fig. 9(b), two critical motors are correctly identified, along with one over-identification, which does not prevent the system from achieving recovery. Once the DSA confirms the consistency between the outputs of both models, the ALSS can be activated. As illustrated in both Figs. 8(c) and 9(c), the system recovers stability after application of corrective control actions through the ALSS. These results demonstrate the adaptability of the proposed approach, as it can adjust

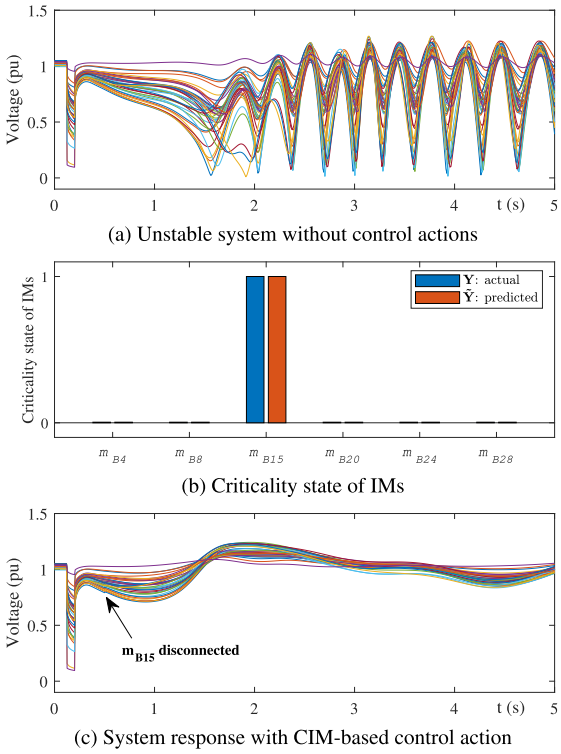

(a) Unstable system without control actions

(b) Criticality state of IMs

(c) System response with CIM-based control action

FIGURE 8. System stabilization result for a test sample: example 1.

the amount and location of motor load shedding required to effectively stabilize different scenarios under STVS conditions.

Finally, a misclassified example was randomly selected to analyze the possible causes of performance gaps in the RCNN models. Fig. 10 shows the voltage responses of all buses following a 3-phase fault located at bus 16–17 in Fig. 5. As can be observed, the system successfully stabilizes after fault clearance, then the expected RCNN outputs should have been ($\tilde{y} = 0; \tilde{\boldsymbol{Y}} = \emptyset$) with an ADS state output as *safe*. However, the actual responses of the RCNN models were ($\tilde{y} = 2; \tilde{\boldsymbol{Y}} = \emptyset$). This means that the STSS-RCNN incorrectly identified a STVS instability, whereas the CIM-RCNN correctly did not identify any critical motors. This disagreement between the models led the ADS output state as *inconsistent*, in which the ALSS is not activated. Although this non-activation was correct, such situations negatively affect the overall performance metrics of the RCNN models.

As illustrated in Fig. 10, the voltage responses in some buses reveal the presence of a phenomenon within STVS known as FIDVR. This phenomenon occurs due to the IM stalling after a fault event, which increases their reactive power demand from the grid and consequently delays the voltage recovery. If the system is unable to provide the necessary reactive power support, FIDVR conditions may lead to voltage collapse and several cascading events [36].

Since the RCNN models were trained to detect the most critical STVS phenomenon (fast voltage collapse), FIDVR

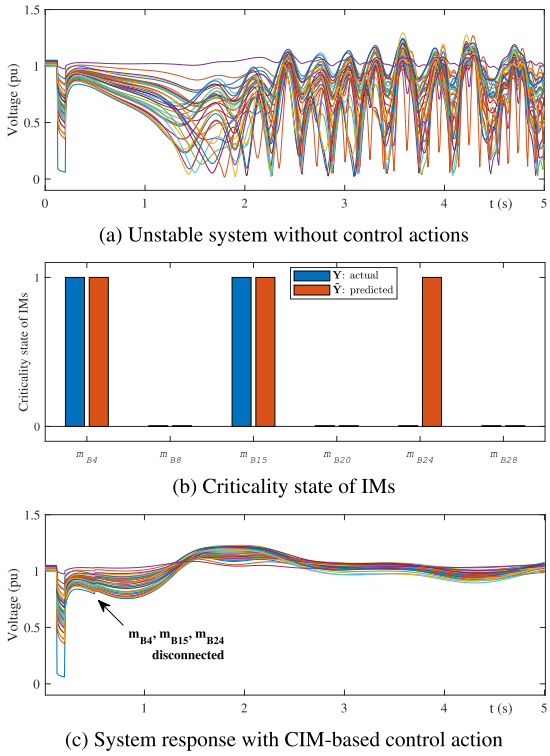

FIGURE 9. System stabilization result for a test sample: example 2.

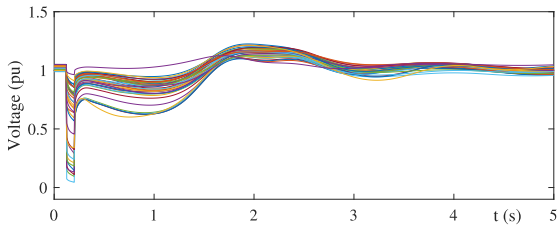

FIGURE 10. RCNN misclassification example: voltage responses exhibiting FIDVR phenomenon.

conditions are not expected to be identified as unstable. However, these stable yet delayed-recovery conditions can still challenge the models discrimination capability, leading to a degradation in classification performance under FIDVR scenarios. To address this challenge, future work could extend the proposed methodology to enable the assessment and control of FIDVR phenomena. The STSS-RCNN model would need to incorporate FIDVR labels based on voltage recovery criteria defined in standards such as WECC/NERC [37]. Likewise, the CIM-RCNN model should include labels for critical motors in FIDVR cases, ensuring that their disconnection leads to voltage recovery consistent with the required transient recovery criteria.

2) COMPARISON WITH OTHERS MODELS

To demonstrate the performance advantage of the trained RCNN models, comparative tests were conducted against the single DL methods that constitute the RCNN model i.e., CNN and LSTM. In this sense, both single DL methods were trained, directly using the multidimensional time series input x as it has dimensional compatibility with both CNN and LSTM. Moreover, the training was carried out in the same way as described in the flowchart in Fig. 1.

TABLE 4. Performance comparison with single DL methods.

	Task 1: STSS-RCNN				Task 2: CIM-RCNN		
Method	Acc	Ss	Cu	Gmean	Jacc	Jaccu	Jacceu
LSTM	97.26	97.34	96.98	97.16	97.33	95.13	96.56
CNN	97.86	97.55	97.31	97.43	97.91	96.17	97.26
RCNN	98.20	98.09	99.26	98.67	98.87	97.60	98.60

TABLE 5. Performance results under noise conditions.

	Task 1: STSS-RCNN				Task 2: CIM-RCNN		
SNR (dB)	Acc	Ss	Cu	Gmean	Jacc	Jaccu	Jacceu
20	97.11	96.49	98.34	97.41	97.44	92.63	95.06
30	97.88	97.66	98.52	98.09	98.69	95.45	97.59
40	98.05	97.66	99.03	98.34	98.84	96.72	98.11
Ideal	98.20	98.09	99.26	98.67	98.87	97.60	98.60

The performances obtained on the test data for CNN and LSTM are presented in Table 4. As shown, both single DL methods achieved excellent results in the two classification tasks, with metrics above 95%. Nonetheless, the proposed RCNN models perform better, as they correctly identify more cases in both STSS and CIM tasks, demonstrating the advantage of combining the individual capabilities of CNN and LSTM.

D. ROBUSTNESS ANALYSIS

To verify the performance of the proposed models, different tests were conducted under adverse conditions in PMU data acquisition, that is, scenarios in which the models receive data with noise or missing measurements.

1) NOISE

In practice, measurements from PMU devices may exhibit a certain degree of distortion, either due to load fluctuations or inherent measurement errors. These effects are generally considered as noise in the signals, whose quantification is performed using the signal-to-noise ratio (SNR). A lower SNR value indicates a higher level of noise distortion in the signal. In this context, different SNR levels were added to the input data x in the test dataset to assess the impact of signal degradation on the performance of the proposed models. The results are summarized in Table 5.

As shown in Table 5, all metrics exhibit a slight decrease compared to the ideal noise-free condition. Even under the extreme condition of 20 dB, the Cu and *G*mean metrics in Task 1 decrease by approximately 1%, while Jaccu and Jacceu in Task 2 show slightly larger reductions of 3% and

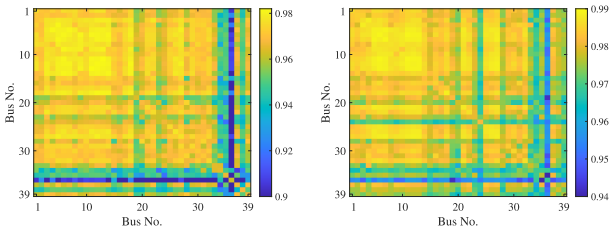

(a) G-mean (b) Jacc

FIGURE 11. Performance results on test dataset under measurement loss.

TABLE 6. Performance results under different time-window length.

	Task 1: STSS-RCNN				Task 2: CIM-RCNN		
t_W	Acc	Ss	Cu	Gmean	Jacc	Jaccu	Jacceu
0.10 s	96.94	96.83	97.31	97.07	97.22	95.22	96.20
0.11 s	97.23	97.12	98.28	97.70	97.89	96.73	97.62
0.12 s	97.42	97.31	98.57	97.94	98.09	96.92	97.82
0.13 s	97.81	97.70	98.96	98.33	98.48	97.31	98.21
0.14 s	98.20	98.09	99.26	98.67	98.87	97.60	98.60

2%, respectively, due to the higher number of prediction labels. In other words, the proposed approach demonstrates a desirable robustness to PMU measurement noise, even under extreme scenarios, maintaining performance levels above 95%.

2) MEASUREMENT LOSS

The performance results shown in Table 3 are based on an ideal scenario where measurements from all system buses are always available. However, in practice, some of these measurements may be missing due to measurement loss or communication failures. In this context, the performance of the STSS-RCNN and CIM-RCNN models is analyzed under the unavailability of PMU measurements at different system buses.

In this context, scenarios involving the loss of PMU measurements in one bus (p-1) or two buses (p-2) were considered. In the test dataset, the time series data for buses without measurements were replaced with the average values of adjacent buses. Using these modified inputs, the RCNN models were evaluated, and the performance results are presented in the heatmap of Fig. 11. In this figure, the horizontal and vertical axes correspond to the buses where measurements are missing, and the color of each cell indicates the performance range of the models. Cells along the diagonal represent performance under p-1 measurement loss (single bus), while the off-diagonal cells correspond to performance under p-2 measurement loss (two buses).

As shown in Fig. 11(a), the performance of Task 1, evaluated using the representative *G*mean metric, remains above 90% for any combination of p-2 and p-1 measurement loss scenarios, and exceeds 94% in most cases. The lowest performance is observed when measurement losses involve a combination of any bus with one of the motor buses 20 or 24, or one of the generator buses 33 to 39, particularly bus 36. In contrast, when measurement losses occur in any combination of non-motor or non-generation buses, the performance is notably higher. Therefore, it can be concluded that measurements in generation and motor buses are especially important to maintain model performance without significant degradation.

Similarly, as shown in Fig. 11(b), where the performance of Task 2 is evaluated using the Jacc metric, the results remain above 94%. In this case, it is also evident that the combination of measurement loss involving any bus and a motor bus (particularly 15, 20 or 24), or a generator bus (particularly 33 - 36), leads to a performance degradation. These results highlight the importance of ensuring measurements at both generator and motor load buses. Although performance decreases in the presence of measurement losses, both models still achieve competitive results, especially when the affected buses are neither motor load nor generator buses.

Therefore, it is demonstrated that the STSS-RCNN and CIM-RCNN models, even under adverse conditions such as noise or missing measurements, maintain competitive performance, enabling in most cases the correct activation of the ALSS.

E. SENSIBILITY ANALYSIS

The RCNN models were developed using a specific window length for the input data and assuming PMU measurement across all system buses. To verify that these conditions indeed provide the best performance and enable the timely activation of corrective actions, a sensitivity analysis was conducted by training the models under alternative input configurations.

1) TIME-WINDOW LENGTH

The time window length t_W required by the models for both classification tasks was defined to ensure both high performance and early instability detection, thus allowing timely control actions. Following this criterion, a value of $t_W = 0.14$ s was set, comprising the fault duration ($t_f = 0.10$ s) plus a short additional margin ($t_m = 0.04$ s). Under this setting, the models achieved performance metrics around 98% in both tasks (Table 3).

To confirm that the adjusted value indeed corresponds to the best performance, systematic experiments were conducted by training the models with different window lengths: 0.10 s ($T = 11$ samples, considering only t_f), 0.11 s ($T = 12$ samples), 0.12 s ($T = 13$ samples), 0.13 s ($T = 14$ samples), and 0.14 s ($T = 15$ samples, the initially adjusted value). The performance results on the test dataset are summarized in Table 6.

From the results in Table 6, it can be observed that as the time window length increases, performance metrics tend to improve, particularly when the time window exceeds the fault duration. The highest results in both tasks, above 98%, are achieved with time window lengths of 0.13 s

TABLE 7. Performance results under different input data location.

	Task 1: STSS-RCNN				Task 2: CIM-RCNN		
Buses	Acc	Ss	Cu	Gmean	Jacc	Jaccu	Jacceu
6	97.38	95.93	98.94	97.42	97.51	91.48	93.00
10	91.57	89.47	93.94	91.68	93.97	90.67	91.01
16	98.04	99.05	99.16	99.10	98.67	97.10	98.43
39 (Ideal)	98.20	98.09	99.26	98.67	98.87	97.60	98.60

and 0.14 s. Although a time window of 0.13 s provides a slightly larger margin for the execution of control actions (inherent latencies), the 0.14 s time window is preferred. This time window not only delivers the best performance but also ensures early detection and timely activation of control actions.

Furthermore, the results show that even with the shortest window (0.10 s, corresponding only to the fault duration), the minimum performance remains above 95% across all metrics for both models. This confirms that even with a few input data samples, the models consistently achieve competitive classification performance.

2) INPUT DATA LOCATION

The RCNN models were initially developed under the assumption that PMU measurements were available at all system buses; however, in practice, this is rarely the case. In this sense, the models were trained using data only from buses particularly relevant to this study: motor load buses and generator buses. These buses closely capture the mechanisms of short-term instability and also highlight their importance for model performance, as shown in Section IV-D. In this context, instead of using data from all $B = 39$ system buses, only generation and motor load buses ($B = 16$) are considered. Additionally, test experiments were conducted by training the models using only generation buses ($B = 10$), and only motor load buses ($B = 6$). Table 7 summarizes the performance results on the test dataset.

The results in Table 7 show that when the models are trained with data from generation and motor load buses ($B = 16$), their performance decreases slightly compared to the ideal case ($B = 39$). This confirms that measurements at these buses are essential for achieving high accuracy. When training is performed using only motor load buses ($B = 6$), the metrics for Task 1 remain above 97%, while in Task 2 they exhibit a reduction, but still reaching competitive performance above 91.5%. In contrast, when only generation buses are used ($B = 10$), the metrics drop by about 8% in both tasks, with values around 90%. At first glance, it may be assumed that using $B = 10$ measurements would yield better performance than using only $B = 6$. However, the results show the opposite. This may be because the number of available measurements is less critical than the locations from which the information is extracted. By collecting data from the six buses where the induction motors (IMs) are located, which includes their speed response ω, solid information is obtained to assess both STSS and CIM, and thereby achieving competitive performance.

In general, these results demonstrate the importance of generation and motor load buses measurements. Therefore, in scenarios with limited PMU devises, it is advisable to prioritize PMU placement at these buses to ensure reliable performance in both STSS assessment and CIM identification.

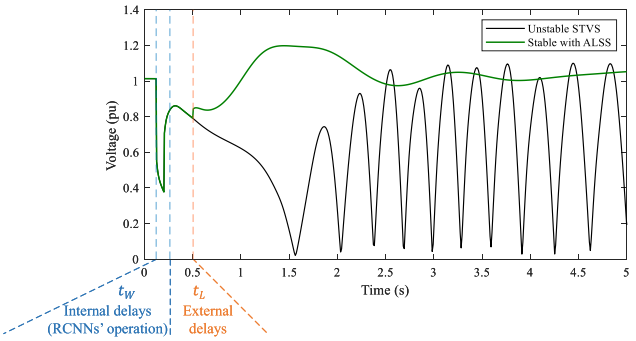

FIGURE 12. Time delays for the enhancement of an unstable STVS sample.

F. REAL-TIME APPLICATION

The real-time application of the proposed methodology requires considering both the time associated with models' task classification (internal delays) and the execution of control actions (external delays). Internal delays correspond to the time required by the RCNN models to predict STSS and CIM ($t_W = 0.14$ s). External delays, on the other hand, involve factors inherent to real-time operation ($t_L < 0.26$ s), including: 1) online computational delays, which depend on the available processing capacity (in this case, ≤ 0.01 s); 2) PMU-based data acquisition (≤ 0.01 s [33]); 3) communication latency from local PMUs to the WAMS central station (≤ 0.15 s [33]); 4) transfer of the control signal from the WAMS central station to motor loads (≤ 0.05 s [34]); and 5) circuit breaker actuation (≤ 0.04 s [35]).

Overall, the total time required by the proposed real-time application is $t_W + t_L \leq 0.4$ s, which is sufficient to mitigate voltage instability issues in a timely manner. Fig. 12 illustrates this behavior, showing how the ALSS successfully mitigates instability in a randomly selected test case and highlights the required delays (t_W and t_L) needed to prevent its development.

G. ALSS AND CONVENTIONAL UVLS

To demonstrate the usefulness and effectiveness of the proposed methodology, a comparison between the proposed ALSS and the classical UVLS (under voltage load shedding) scheme was developed. The UVLS scheme is designed to prevent the system from entering collapse conditions and to maintain voltage within acceptable levels after a

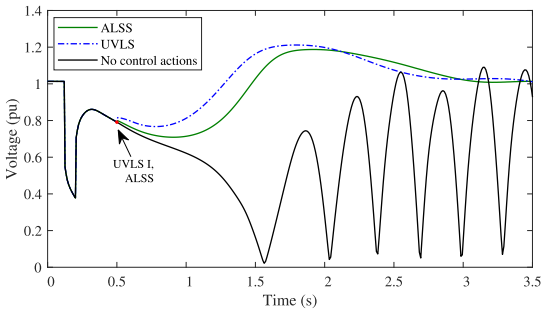

(a) Voltage responses at bus 16 under ALSS and UVLS activation for an unstable STVS sample

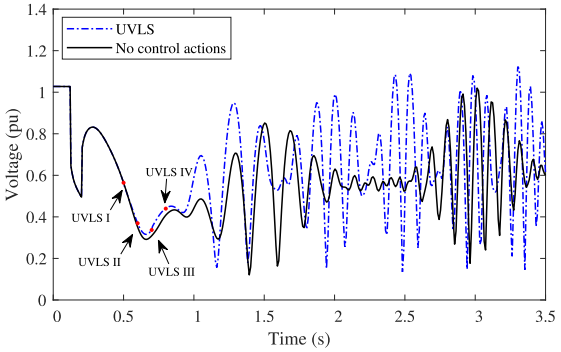

(b) Voltage responses at bus 17 under UVLS activation for an unstable TS sample

FIGURE 13. ALSS and UVLS comparision.

disturbance [38]. The design of UVLS relies on predefined disturbances and predetermined operating scenarios, whose parameters are set through offline simulations and the experience of protection and planning engineers [38]. In general, the UVLS activation is conducted by standard criteria, such as the transient voltage recovery criteria (TVRC) proposed by WECC/NERC [37], which establishes acceptable voltage limits and recovery times following a disturbance. In addition, the load shedding process is implemented in successive stages, with different percentages of load and time delays, applied at buses with the largest voltage deviations.

In particular, the TVRC specifies that if the voltage profile remains below 0.8 pu for more than 20 cycles, the UVLS scheme must be activated. This criterion allows the scheme to detect not only fast voltage collapse risks but also phenomena such as FIDVR and sustained low voltage. Typically, the disconnection process is defined in four stages: 1) 10% load shedding at 0.05 s after fault clearing; (2) 5% load shedding at 0.15 s after fault clearing; (3) 5% load shedding at 0.25 s after fault clearing; and (4) 5% load shedding at 0.35 s after fault clearing. Note that these disconnection times do not consider external delays associated with the execution of control actions, which must be included to realistically assess the response of the scheme.

Fig. 13 presents two representative cases, one involving STVS instability and another related to TS instability, where

TABLE 8. UVLS and ALSS application results.

Sample	Scheme	Activation	LS amount
Unstable by STVS	UVLS	TVRC	9.74 %
	ALSS	*Critical − STVS*	1.32 %
Unstable by TS	UVLS	TVRC	25 %
	ALSS	–	–

the UVLS and ALSS schemes are compared. In addition, Table 8 summarizes the results obtained for each scheme (activation criteria and load shedding parameters).

The STVS event was developed after a 3-phase fault on transmission line 17-18 in Fig. 5. As shown in Fig. 13(a), both schemes successfully mitigated the instability according to their respective criteria. TVRC for the UVLS scheme and *critical − STVS* for ALSS (RCNN responses: $\tilde{y} = 2, \tilde{\boldsymbol{Y}} \neq \emptyset$). In the case of UVLS, only one stage was required since the voltage remained above 0.8 pu after the control execution. However, this single stage involved shedding 10% of the total system load, whereas the proposed ALSS scheme only shed 1.32% (see Table 8).

In contrast, for the transient instability case produced after a 3-phase fault on transmission line 21–22 in Fig. 5, only the UVLS scheme is activated, as shown in Fig. 13(b). This occurs because the voltage response fails to recover within the limits defined by the TVRC; consequently, all four load-shedding stages are executed (25% of the total load). Nevertheless, the system fails to recover stability, as this is an inherently unstable TS sample in which the instability mechanism corresponds to generator out-of-step rather than motor dynamics, making load shedding ineffective. The proposed ALSS scheme does not activate due to the RCNN model responses ($\tilde{y} = 1, \tilde{\boldsymbol{Y}} = \emptyset$), thereby confirming its correct non-activation.

Overall, these results highlight the superiority of the proposed ALSS, as it not only activates precisely and in a timely manner but also adapts its control actions to the mechanism that originates STVS events, namely the critical motor load.

V. DISCUSSIONS

The mechanism behind STVS instability originates from the IM stalling during transient processes following contingency events. This situation is reflected in variations of motor speed (ω), voltage (V), and reactive power (Q). After a fault, the motors decelerate while seeking a new equilibrium between electromagnetic and mechanical torques, drawing high currents and reactive power [2]. The RCNN models are capable of capturing information from the motors during transient process through the selected input variables (V, ω). The inclusion of ω together with V implies that the Q is considered ($Q = f(V, \omega)$). Therefore, the nonlinear interactions between these variables that occur during the transient period can be inferred by the RCNN models without

being explicitly modeled, enabling predictive identification of the most critical STVS phenomenon — fast voltage collapse.

Additionally, it should be noted that as the RCNN are designed to operate within the short-term time frame upon the occurrence of large failure, the excitation system dynamics response remains in its transient range and does not reach its long-term limits. Therefore, the models primarily capture the fast interactions among the input variables that characterize STVS and TS. As a result, the RCNN is not affected by long-term interdependencies but rather learns to identify the rapid dynamic patterns associated with motor stalling and generator out-of-step.

On the other hand, the methodology assumes that the time series data responses obtained from dynamic simulations closely represent the actual behavior of the system. In other words, a high accuracy level in the dynamic modeling, particularly of generators and motors, is required.

Regarding model retraining, this becomes necessary only when significant changes occur in the system topology, for example, the addition or removal of transmission lines, generators, or other major system components that substantially alter the dynamic behavior of the system. In contrast, retraining is not required for variations in demand or generation dispatch since the database already accounts for such conditions through the inclusion of multiple load/generation scenarios.

Finally, it is worth noting that improving generalization to unseen disturbances requires increasing the diversity of the training database. Incorporating additional contingencies types, such as high-impedance faults or different fault configurations (single-phase or two-phase faults), would expose the models to a wider range of dynamic responses. This enhanced variability enables the models to learn more robust features and extend their applicability to a broader set of disturbances.

VI. CONCLUSION

To address STVS instability, this work proposes an integrated assessment methodology of STSS and CIM for the effective activation and guidance of control actions within an ALSS framework. The data-driven assessment of STSS and CIM enables the early prediction of stability conditions and identification of critical loads after a contingency, allowing ALSS to be activated in a timely manner and to adapt its control actions for system stabilization.

Leveraging the RCNN algorithm, which captures both spatial and temporal features from system variables, the proposed STSS-RCNN and CIM-RCNN models achieved high performance suitable for real-time applications. Numerical results on the IEEE 39-bus test system demonstrated that the proposed approach accurately predicts both STSS and CIM, enabling adaptive and timely control measures to mitigate potential STVS events. Furthermore, the models proved robust to measurement loss and noise, and outperformed approaches based on single DL methods, reinforcing their reliability for practical implementation. In addition, the proposed ALSS demonstrated its superiority to a traditional UVLS scheme thanks to its more precise activation and adaptive critical motor load shedding, achieving system stabilization with a significantly lower demand reduction.

In future work, research efforts will focus on extending the proposed framework to FIDVR scenarios and integrating specific control actions to address TS-related issues (e.g. generation tripping). In addition, alternative architectural choices will be explored to enhance data-driven STSS and CIM assessment. The methodology will be applied to real systems with high renewable energy penetration and validated through real-time simulations using an RTDS platform. This will further enhance its applicability and relevance for modern power system operation.

REFERENCES

[1] M. Glavic, D. Novosel, E. Heredia, D. Kosterev, A. Salazar, F. Habibi-Ashrafi, and M. Donnelly, "See it fast to keep calm: Real-time voltage control under stressed conditions," *IEEE Power Energy Mag.*, vol. 10, no. 4, pp. 43–55, Jul. 2012.

[2] J. A. D. D. Leon and C. W. Taylor, "Understanding and solving short-term voltage stability problems," in *Proc. IEEE Power Eng. Soc. Summer Meeting*, vol. 2, Jul. 2003, pp. 745–752.

[3] C. W. Taylor, "Concepts of undervoltage load shedding for voltage stability," *IEEE Trans. Power Del.*, vol. 7, no. 2, pp. 480–488, Apr. 1992.

[4] J. Wang, H. Zhang, and Y. Zhou, "Intelligent under frequency and under voltage load shedding method based on the active participation of smart appliances," *IEEE Trans. Smart Grid*, vol. 8, no. 1, pp. 353–361, Jan. 2017.

[5] I. Goodfellow, Y. Bengio, A. Courville, and Y. Bengio, *Deep Learning*, vol. 1. Cambridge, MA, USA: MIT Press, 2016.

[6] H. Yang, W. Zhang, J. Chen, and L. Wang, "PMU-based voltage stability prediction using least square support vector machine with online learning," *Electric Power Syst. Res.*, vol. 160, pp. 234–242, Jul. 2018.

[7] Y. Xu, R. Zhang, J. Zhao, Z. Y. Dong, D. Wang, H. Yang, and K. P. Wong, "Assessing short-term voltage stability of electric power systems by a hierarchical intelligent system," *IEEE Trans. Neural Netw. Learn. Syst.*, vol. 27, no. 8, pp. 1686–1696, Aug. 2016.

[8] Y. Zhang, Y. Xu, Z. Y. Dong, and R. Zhang, "A hierarchical self-adaptive data-analytics method for real-time power system short-term voltage stability assessment," *IEEE Trans. Ind. Informat.*, vol. 15, no. 1, pp. 74–84, Jan. 2019.

[9] J. D. Pinzón and D. G. Colomé, "Real-time multi-state classification of short-term voltage stability based on multivariate time series machine learning," *Int. J. Electr. Power Energy Syst.*, vol. 108, pp. 402–414, Jun. 2019.

[10] H. Hagmar, L. Tong, R. Eriksson, and L. A. Tuan, "Voltage instability prediction using a deep recurrent neural network," *IEEE Trans. Power Syst.*, vol. 36, no. 1, pp. 17–27, Jan. 2021.

[11] S. M. H. Rizvi, S. K. Sadanandan, and A. K. Srivastava, "Data-driven short-term voltage stability assessment using convolutional neural networks considering data anomalies and localization," *IEEE Access*, vol. 9, pp. 128345–128358, 2021.

[12] A. Adhikari, S. Naetiladdanon, and A. Sangswang, "Real-time short-term voltage stability assessment using combined temporal convolutional neural network and long short-term memory neural network," *Appl. Sci.*, vol. 12, no. 13, p. 6333, Jun. 2022.

[13] G. Wang, Z. Zhang, Z. Bian, and Z. Xu, "A short-term voltage stability online prediction method based on graph convolutional networks and long short-term memory networks," *Int. J. Electr. Power Energy Syst.*, vol. 127, May 2021, Art. no. 106647.

[14] Y. Luo, C. Lu, L. Zhu, and J. Song, "Data-driven short-term voltage stability assessment based on spatial–temporal graph convolutional network," *Int. J. Electr. Power Energy Syst.*, vol. 130, Sep. 2021, Art. no. 106753.

[15] Y. Li, S. Zhang, Y. Li, J. Cao, and S. Jia, "PMU measurements-based short-term voltage stability assessment of power systems via deep transfer learning," *IEEE Trans. Instrum. Meas.*, vol. 72, pp. 1–11, 2023.

[16] Y. Li, J. Cao, Y. Xu, L. Zhu, and Z. Y. Dong, "Deep learning based on transformer architecture for power system short-term voltage stability assessment with class imbalance," *Renew. Sustain. Energy Rev.*, vol. 189, Jan. 2024, Art. no. 113913.
[17] E. G. Potamianakis and C. D. Vournas, "Short-term voltage instability: Effects on synchronous and induction machines," *IEEE Trans. Power Syst.*, vol. 21, no. 2, pp. 791–798, May 2006.
[18] T. Van Cutsem and C. Vournas, *Voltage Stability of Electric Power Systems*. Cham, Switzerland: Springer, 2007.
[19] H. Ge, Q. Guo, H. Sun, and W. Zhao, "A model and data hybrid-driven short-term voltage stability real-time monitoring method," *Int. J. Electr. Power Energy Syst.*, vol. 114, Jan. 2020, Art. no. 105373.
[20] M. Lashgari and S. M. Shahrtash, "Fast online decision tree-based scheme for predicting transient and short-term voltage stability status and determining driving force of instability," *Int. J. Electr. Power Energy Syst.*, vol. 137, May 2022, Art. no. 107738.
[21] E. A. Tapia, D. G. Colomé, and J. L. Rueda Torres, "Recurrent convolutional neural network-based assessment of power system transient stability and short-term voltage stability," *Energies*, vol. 15, no. 23, p. 9240, Dec. 2022.
[22] H. Bai and V. Ajjarapu, "A novel online load shedding strategy for mitigating fault-induced delayed voltage recovery," *IEEE Trans. Power Syst.*, vol. 26, no. 1, pp. 294–304, Feb. 2011.
[23] Y. Dong, X. Xie, K. Wang, B. Zhou, and Q. Jiang, "An emergency-demand-response based under speed load shedding scheme to improve short-term voltage stability," *IEEE Trans. Power Syst.*, vol. 32, no. 5, pp. 3726–3735, Sep. 2017.
[24] M. Ghotbi-Maleki, R. M. Chabanloo, and H. Javadi, "Load shedding strategy using online voltage estimation process for mitigating fault-induced delayed voltage recovery in smart networks," *Electric Power Syst. Res.*, vol. 214, Jan. 2023, Art. no. 108899.
[25] T. B. Nguyen and M. A. Pai, "Dynamic security-constrained rescheduling of power systems using trajectory sensitivities," *IEEE Trans. Power Syst.*, vol. 18, no. 2, pp. 848–854, May 2003.
[26] J. C. Cepeda and D. G. Colomé, "Evaluación de la vulnerabilidad del sistema eléctrico de potencia en tiempo real usando tecnología de medición sincrofasorial," *Revista Técnica Energía*, vol. 10, no. 1, pp. 91–101, Jan. 2014.
[27] M. Massaoudi, H. Abu-Rub, S. S. Refaat, I. Chihi, and F. S. Oueslati, "Deep learning in smart grid technology: A review of recent advancements and future prospects," *IEEE Access*, vol. 9, pp. 54558–54578, 2021.
[28] S. Hochreiter and J. Schmidhuber, "Long short-term memory," *Neural Comput.*, vol. 9, no. 8, pp. 1735–1780, Nov. 1997.
[29] J. Huang, L. Guan, Y. Su, H. Yao, M. Guo, and Z. Zhong, "Recurrent graph convolutional network-based multi-task transient stability assessment framework in power system," *IEEE Access*, vol. 8, pp. 93283–93296, 2020.
[30] D. P. Kingma and J. Ba, "Adam: A method for stochastic optimization," 2014, *arXiv:1412.6980*.
[31] H. Gouk, B. Pfahringer, and M. J. Cree, "Learning distance metrics for multi-label classification," in *Proc. Asian Conf. Mach. Learn.*, vol. 63, 2016, pp. 318–333.
[32] A. Pai, *Energy Function Analysis for Power System Stability*. Cham, Switzerland: Springer, 1989.
[33] U. Rudez and R. Mihalic, "WAMS-based underfrequency load shedding with short-term frequency prediction," *IEEE Trans. Power Del.*, vol. 31, no. 4, pp. 1912–1920, Aug. 2016.
[34] P. Kansal and A. Bose, "Bandwidth and latency requirements for smart transmission grid applications," *IEEE Trans. Smart Grid*, vol. 3, no. 3, pp. 1344–1352, Sep. 2012.
[35] A. Abb, "Live tank circuit breakers-buyers guide," ABB AG, Tech. Rep., 2008. [Online]. Available: https://aitcorp.com.vn/images/ckeditor/files/abb/2_Catalogue%20CB%20110kV.pdf
[36] G. K. Stefopoulos and A. P. Meliopoulos, "Induction motor load dynamics: Impact on voltage recovery phenomena," in *Proc. PES TD*, 2006, pp. 752–759.
[37] B. Gong, D. Kosterev, J. Eto, J. Undrill, K. Sreenivasachar, O. Lutalo, P. Mitra, S. Wang, and V. Vittal, "Whitepaper on transient voltage response criteria," in *Proc. NERC*, 2022, pp. 1–48.
[38] C. J. Mozina, "Undervoltage load shedding," in *Proc. 60th Annu. Conf. Protective Relay Engineers*, Mar. 2007, pp. 16–34.

ESTEFANÍA A. TAPIA SUÁREZ received the B.S. degree in electrical engineering from the Escuela Politécnica Nacional, Quito, Ecuador, in 2015, and the Ph.D. degree in electrical engineering from the National University of San Juan, Argentina, in 2023. From 2023 to 2025, she was a Researcher in artificial intelligence and data processing with the AIMEN Technology Centre, Vigo, Spain. She is currently a Postdoctoral Research Associate with Delft University of Technology, The Netherlands. Her research interests include the assessment and control of power system stability, the application of artificial intelligence to power systems, and the integration of renewable energy.

D. GRACIELA COLOMÉ received the Ph.D. degree in electrical engineering from the National University of San Juan (UNSJ), Argentina, in 2009. From 2011 to 2018, she was a Coordinator of the Electrical Engineering Program. From 2016 to 2021, she was the Director of the Graduate Studies Department, School of Engineering, UNSJ. She is currently a Professor and a Consultant with the Institute of Electric Energy (IEE), UNSJ–CONICET, where she also leads research and technology transfer projects. Her research interests include modeling, simulation, supervision, stability, and control of electrical power systems.

JOSÉ L. RUEDA TORRES (Senior Member, IEEE) was born in 1980. He received the Electrical Engineering Diploma degree (cum laude) from the Escuela Politécnica Nacional, Quito, Ecuador, in August 2004, and the Ph.D. degree (Sobresaliente) in electrical engineering from the National University of San Juan, in November 2009. From September 2003 to February 2005, he was in Ecuador, involved in the fields of industrial control systems and electrical distribution networks operation and planning. From August 2010 to February 2014, he was a Postdoctoral Research Associate with the Institute of Electrical Power Systems, University of Duisburg-Essen, Duisburg, Germany. He is currently an Associate Professor leading the Research Team on Dynamic Stability of Sustainable Electrical Power Systems, Intelligent Electrical Power Grids Section, Electrical Sustainable Energy Department, Delft University of Technology, Delft, The Netherlands. His research interests include physics-driven analysis of stability phenomena dynamic equivalencing of HVDC-HVAC systems, probabilistic multi-systemic reliability, and stability management, and adaptive-optimal resilient multi-objective controller design. He is a member of the Technical Committee on Power and Energy Systems of the International Federation of Automatic Control (IFAC), the Vice-Chair of the IEEE PES Intelligent Systems Subcommittee, and the Vice-Chair of the IFAC Technical Committee TC 6.3. Power and Energy Systems on social media.